

# CHEMICAL COMPLEXITY IN LOCAL DIFFUSE AND TRANSLUCENT CLOUDS: UBIQUITOUS LINEAR-C<sub>3</sub>H AND CH<sub>3</sub>CN, A DETECTION OF HC<sub>3</sub>N AND AN UPPER LIMIT ON THE ABUNDANCE OF CH<sub>2</sub>CN

HARVEY LISZT

National Radio Astronomy Observatory  
520 Edgemont Road, Charlottesville, VA 22903-2475  
hliszt@nrao.edu

MARYVONNE GERIN

LERMA, Observatoire de Paris, PSL Research University,  
CNRS, Sorbonne Université, UPMC Université Paris 06,  
Ecole Normale Supérieure, 75005, Paris, France  
gerin@lra.ens.fr

ANTHONY BEASLEY

National Radio Astronomy Observatory  
520 Edgemont Road, Charlottesville, VA 22903-2475  
tbeasley@nrao.edu

JEROME PETY

Institut de Radioastronomie Millimétrique, 300 Rue de la Piscine, F-38406 Saint Martin d'Hères, France  
CNRS, Sorbonne Université, UPMC Université Paris 06,  
Ecole Normale Supérieure, 75005, Paris, France  
pety@iram.fr

## ABSTRACT

We present Jansky Very Large Array observations of 20 - 37 GHz absorption lines from nearby Galactic diffuse molecular gas seen against four cosmologically-distant compact radio continuum sources. The main new observational results are that *l*-C<sub>3</sub>H and CH<sub>3</sub>CN are ubiquitous in the local diffuse molecular interstellar medium at  $A_V \lesssim 1$  while HC<sub>3</sub>N was seen only toward B0415 at  $A_V > 4$  mag. The linear/cyclic ratio is much larger in C<sub>3</sub>H than in C<sub>3</sub>H<sub>2</sub> and the ratio CH<sub>3</sub>CN/HCN is enhanced compared to TMC-1, although not as much as toward the Horsehead Nebula. More consequentially, this work completes a long-term program assessing the abundances of small hydrocarbons (CH, C<sub>2</sub>H, linear and cyclic C<sub>3</sub>H and C<sub>3</sub>H<sub>2</sub>, and C<sub>4</sub>H and C<sub>4</sub>H<sup>-</sup>) and the CN-bearing species (CN, HCN, HNC, HC<sub>3</sub>N, HC<sub>5</sub>N and CH<sub>3</sub>CN): their systematics in diffuse molecular gas are presented in detail here. We also observed but did not strongly constrain the abundances of a few oxygen-bearing species, most prominently HNCO. We set limits on the column density of CH<sub>2</sub>CN, such that the anion CH<sub>2</sub>CN<sup>-</sup> is only viable as a carrier of diffuse interstellar bands if the N(CH<sub>2</sub>CN)/N(CH<sub>2</sub>CN<sup>-</sup>) abundance ratio is much smaller in this species than in any others for which the anion has been observed. We argue that complex organic molecules are not present in clouds meeting a reasonable definition of diffuse molecular gas, ie  $A_V \lesssim 1$  mag.

*Keywords:* astrochemistry . ISM: molecules . ISM: clouds. Galaxy

## 1. INTRODUCTION

The molecular inventory of diffuse interstellar gas is interesting because the unexpectedly high abundances of trace species imply the presence of underlying physical processes that might otherwise remain hidden (Godard et al. 2014). But knowledge of the molecular complement of diffuse molecular gas can be used to advantage even when the underlying

physical processes and observed abundances are only very imperfectly understood:

- Chemistry provides reliable H<sub>2</sub>-tracers with well-determined relative abundances from optical astronomy such as OH ( $X(\text{OH}) = N(\text{OH})/N(\text{H}_2) = 10^{-7}$  (Weselak et al. 2009, 2010)) and CH ( $X(\text{CH}) = 3.5 \times 10^{-8}$  (Sheffer et al. 2008)) as well as HCO<sup>+</sup> that is observed in absorption at 89 GHz with an abundance  $X(\text{HCO}^+) = 3 \times 10^{-9}$  that can be fixed with respect to both CH and OH (Liszt & Lucas 1996; Liszt et al. 2010; Liszt & Gerin 2016).
- The empirically-determined relative abundance of HCO<sup>+</sup> suffices to explain observations of widely-observed CO in diffuse molecular gas (Liszt et al. 2010) as the product of recombination of HCO<sup>+</sup> with ambient electrons (Glassgold & Langer 1975; Liszt 2007; Visser et al. 2009; Liszt 2017) followed by exchange of carbon isotopes (Watson et al. 1976; Liszt 2017).
- Tallying the inventory of identifiable molecular species sets broad guidelines for attributing practicable carriers of diffuse interstellar bands (DIBs) (Liszt et al. 2012, 2014a). We recently showed that *l*-C<sub>3</sub>H<sub>2</sub> is not sufficiently abundant to serve as the carrier of the DIBs at 4881Å and 5450Å with which it was tentatively identified on the basis of coincidences in laboratory spectra (Maier et al. 2011). Constraining the abundance of another putative DIB-carrier, CH<sub>2</sub>CN<sup>-</sup> (Cordiner & Sarre 2007), is one aspect of the present work. Knowledge of the abundances of smaller molecules should help in understanding the abundances of broad groups of much larger species like polycyclic aromatic hydrocarbons (PAHs) that may not be individually identifiable.

The molecular inventory of diffuse molecular gas has recently been greatly enlarged using high spectral resolution heterodyne techniques. The HiFi instrument on HERSCHEL observed an extensive inventory of carbon, oxygen and nitrogen hydrides and hydride ions in the sub-mm and THz domains (Gerin et al. 2016), including species long known in optical absorption (CH, CH<sup>+</sup>) but also such species as hydrofluoric acid (HF) and the argonium ion ArH<sup>+</sup>. CF<sup>+</sup>, *c*-C<sub>3</sub>H and HCO were detected in local gas at the IRAM 30m telescope (Liszt et al. 2014b) and CF<sup>+</sup> was subsequently detected in diffuse molecular gas across the galactic disk (Liszt et al. 2015) using NOEMA.

In this work we were motivated to extend the molecular inventory and explore the limits of chemical complexity in diffuse molecular gas, given the recently-developed spectroscopic capabilities of the enhanced Jansky Very Large Array (VLA). We used the VLA to search at frequencies 20 - 37

GHz for polyatomic molecules whose transitions are most favorably observed in the cm-wave band. We study three chemical families:

- Hydrocarbons. *l*-C<sub>3</sub>H<sub>2</sub> and *c*-C<sub>3</sub>H<sub>2</sub> are the heaviest molecules known in local diffuse molecular gas but they and *c*-C<sub>3</sub>H are as ubiquitous as the lighter hydrocarbons CH and C<sub>2</sub>H: by contrast, C<sub>4</sub>H has not been detected (Liszt et al. 2012, 2014a). Here we demonstrate the ubiquity and high abundance of *l*-C<sub>3</sub>H and compare the abundances of the linear and cyclic versions of C<sub>3</sub>H and C<sub>3</sub>H<sub>2</sub>. Loison et al. (2017) have recently shown that the relative abundance of the linear and cyclic versions of these molecules represents a competition between formation and isomerization by interaction with atomic hydrogen. The abundance of neutral atomic hydrogen is much higher in diffuse molecular gas, presenting an interesting test of the chemistry. Loison et al. (2017) stress the role of C<sub>3</sub>, which is uniquely observable in diffuse molecular gas. Here we show that C<sub>2</sub>, also uniquely observable in diffuse molecular gas, is by a slight margin over CH and C<sub>2</sub>H the most abundant carbon-bearing molecule after CO: this would not have been possible without a comprehensive survey.
- CN-bearing molecules. The relative abundances of CN, HCN and HNC are very nearly constant in diffuse molecular gas (Liszt & Lucas 2001) but larger CN-bearing species have yet to be detected (Liszt et al. 2008). Here we show that CH<sub>3</sub>CN is ubiquitous at A<sub>v</sub> = 1 mag, which is quite a surprise given that recent models of the formation of CH<sub>3</sub>CN at such moderate extinction predicted an abundance of CH<sub>3</sub>CN that is some five orders of magnitude below the observed levels (Majumdar et al. 2014). We also detect HC<sub>3</sub>N toward B0415+379 (3C111) at E<sub>B-V</sub> = 1.6 mag but not toward B2200+420 (BL Lac) at E<sub>B-V</sub> = 0.33 mag (E<sub>B-V</sub> ≈ A<sub>v</sub>/3.1).
- Oxygen-bearing molecules. Previously-detected, lighter oxygen-bearing species include OH, HCO<sup>+</sup>, HOC<sup>+</sup>, HCO and CO observed at radio frequencies, and H<sub>2</sub>O and the many oxygen hydrides and hydride ions observed by HiFi (Gerin et al. 2016). H<sub>2</sub>CO, usually thought to form on dust, is known to be ubiquitous in diffuse molecular gas (Nash 1990; Marscher et al. 1993; Liszt et al. 2006) although CH<sub>3</sub>OH, which must form on grains, is not detected (Liszt et al. 2008). Here we set limits on an eclectic group of heavier oxygen-bearing species HNCO, HCOOH (formic acid) and H<sub>2</sub>COH<sup>+</sup>. The systematics of the oxygen-bearing species are not discussed here, owing to the paucity of significant new results.

The plan of this work is as follows. In Section 2 we describe the new observations discussed here and the manner of the presentation of the results. In Sections 3 - 5 we separately discuss the hydrocarbon, CN-bearing and oxygen-bearing species including results for CH, CN, C<sub>2</sub> and C<sub>3</sub> that are observed in optical/UV absorption along sightlines having comparable E<sub>B-V</sub> and CH to those observed here. Section 6 discusses the viability of CH<sub>2</sub>CN<sup>-</sup> as a DIB carrier, Section 7 compares our results with those of [Thiel et al. \(2017\)](#) for diffuse clouds observed toward Sgr B2 in the Galactic center and disk and Section 8 is a summary.

## 2. OBSERVATIONS, CONVENTIONS AND CONVERSION FROM OPTICAL DEPTH TO COLUMN DENSITY

### 2.1. Observing and data reduction

The new observations reported here were taken at the National Radio Observatory's Very Large Array (VLA) on 17 June and 6 July 2013 under proposal 13A-097 while in the C-configuration having angular resolution 25-45 milliarcsec. The data were taken in four scheduling blocks (SB) of 2 hour duration, observing absorption against the continuum targets listed in Table 1 in two orthogonal polarizations. The observing was done with 8 spectral windows having 512 channels of resolution and separation 78 kHz placed opportunistically within the range 20.1 - 22.5 GHz in June (corresponding to velocity resolution 0.104 - 0.115 km s<sup>-1</sup>) and 512 channels of resolution and separation 156 kHz within the range 32.7 - 37.3 GHz in July, corresponding to velocity resolution 0.126 - 0.143 km s<sup>-1</sup>. Spectroscopic properties of the newly-observed spectral lines discussed here are summarized in Table 2.

As in our earlier project discussed in [Liszt et al. \(2012\)](#), two continuum targets and a bandpass calibrator (3C84) were covered in each SB. Considerable time was devoted to reference pointing on each continuum source before it was observed. No absolute amplitude calibration was performed but the fluxes relative to that of the bandpass calibrator 3C 84 ( $S_\nu \approx 10 - 16$  Jy) are given in Table 1. In each SB the bandpass calibrator was observed for approximately 20 minutes. The sources were observed for approximately 40 minutes during any one SB execution.

The data were calibrated using very standard techniques in CASA, largely repeating the procedures described in [Liszt et al. \(2012\)](#): Overall the scheme resembles that given in online CASA tutorials for spectral line sources such as TW Hydra with the notable exception that each absorption target, being a phase calibrator, serves as its own phase calibrator. The bandpass calibrator observations were phase-calibrated within each scan sub-interval, followed by construction of an average bandpass solution. This was applied on the fly to complex gain-cal solutions for each continuum target at the sub-scan level, followed by scan-length gain cal-

ibration solutions to be applied to each target individually. Once the data were passband- and phase-calibrated in this way they were also fully reduced given the point-like nature of the background targets. For each polarization and baseband, spectra were extracted as vector phase averages over all visibilities, without gridding, mapping or, indeed, more than very minimal manual flagging of bad datapoints. The spectra were produced in CASA's plotms visualizer and exported to drawspect singledish software ([Liszt 1997](#)) where spectra in the two polarizations were co-added and very small linear baselines amounting typically to 0.01% of the continuum were removed from each of the basebands.

All velocities discussed here are relative to the kinematic definition of the Local Standard of Rest that is in universal use at radio telescopes.

### 2.2. Conversion from integrated optical depth to column density

Equivalent widths (integrated optical depths) are given in Table 3. For *l*-C<sub>3</sub>H the entries are the average of the two lines observed. For CH<sub>3</sub>CN the entries for K=0 are the sum of the optical depths of the three K=0 transitions listed in Table 1. The K=0 and K=1 transitions are easily distinguished toward B0415 and B2200 (Figure 4) but not toward B0355, given the complex kinematic structure and modest signal/noise. For B0355 the only quantity given in Table 3 is the integrated optical depth for all kinematic components summed over both K-ladders and the total column density was determined by scaling with respect to the analogous quantity derived toward the sources B2200 and B0415 where the K-ladder structure was resolved.

Default factors needed to convert the observed integrated optical depths (Table 3) to column density (Tables 4-6) are given in the next-to-last column of Table 2: these were computed by assuming rotational excitation in equilibrium with the cosmic microwave background. This is an excellent approximation for strongly-polar diatomics (ie, not CO) and smaller polyatomics having low-J transitions in the mm-wave regime where emission is demonstrably weak, typically a few hundredths of a Kelvin for even optically thick lines ([Lucas & Liszt 1996](#); [Liszt & Pety 2016](#)). However, for lower-lying transitions of heavier species observed at cm-wavelengths as in this work, collisional excitation more efficiently redistributes the rotational population out of the lowest states, increasing the numerical factors that should be used to convert observed optical depths to column density.

An upward correction factor due to rotational excitation is tabulated separately as a range in the right-most column of Table 2, corresponding to results for the density range  $n(\text{H}_2) = 0 - 400$  cm<sup>-3</sup> that is used in Appendix A. The maximum correction is often below 2 but can be larger when the lowest-lying transition was observed. We have kept the default equivalent width - column density conversion separate from application of the excitation correction, in part because

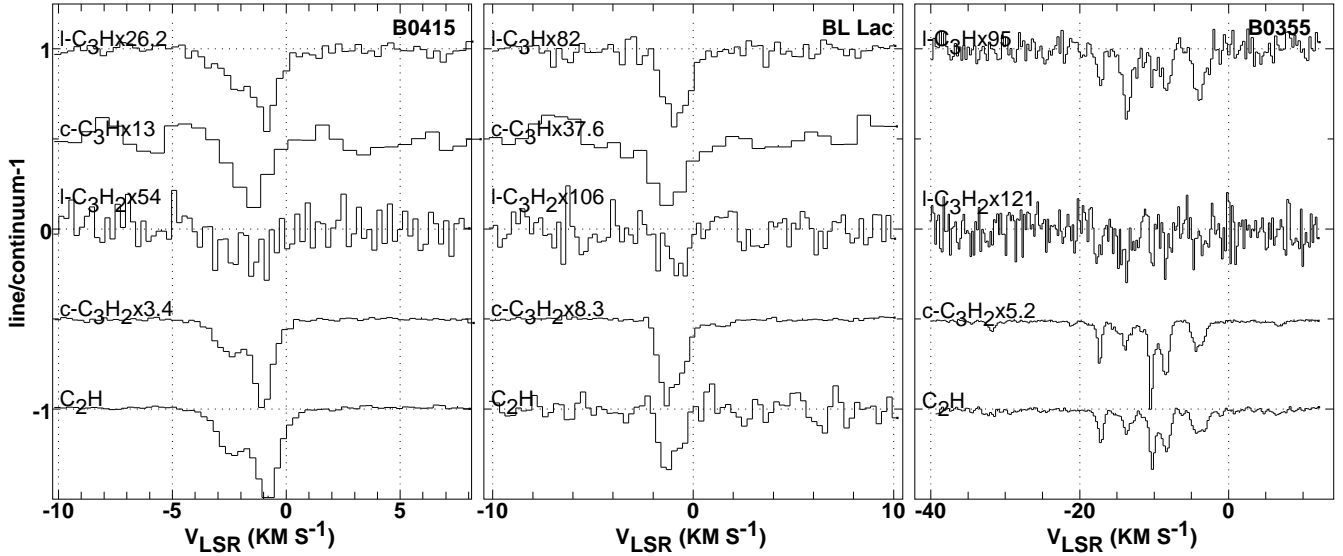


**Figure 1.** Hydrocarbon line profiles toward B0415+379 ,B2200+420 and B0355+508 , vertically displaced and scaled as indicated. The  $l$ - $C_3H$  profiles at the top of each panel are new from this work.  $c$ - $C_3H$  was not observed toward B0355.

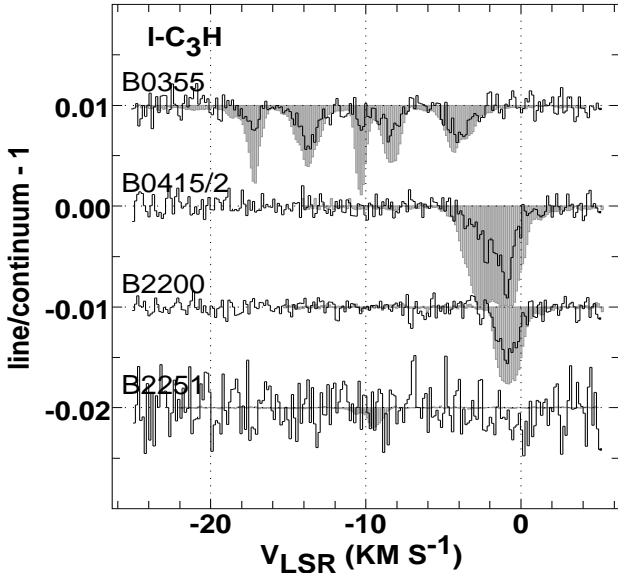


**Figure 2.** Line profiles of  $l$ - $C_3H$  for all sources are shown as histograms compared with profiles of  $HCO^+$  shown shaded in light grey and scaled downward by a factor 100. For B0415 the  $l$ - $C_3H$  profile has been scaled downward by a factor 2.  $HCO^+$  absorption toward B2251+158 is at  $-9.6 \text{ km s}^{-1}$ .

all of the new observations are unlikely to be characterized by the same density, but the correction should be kept in mind during the discussion and it is noted explicitly in the text as required. Throughout, we have avoided drawing conclusions that seemed unwarranted in the face of this uncertainty.

### 2.3. Presentation of results: Figures and tables

Figure 1 shows results for the newly-detected species  $l$ - $C_3H$  along with a complement of spectra of previously-observed hydrocarbons having two and three carbons:  $c$ - $C_3H$  was not observed toward B0355+508 by Liszt et al. (2014b).

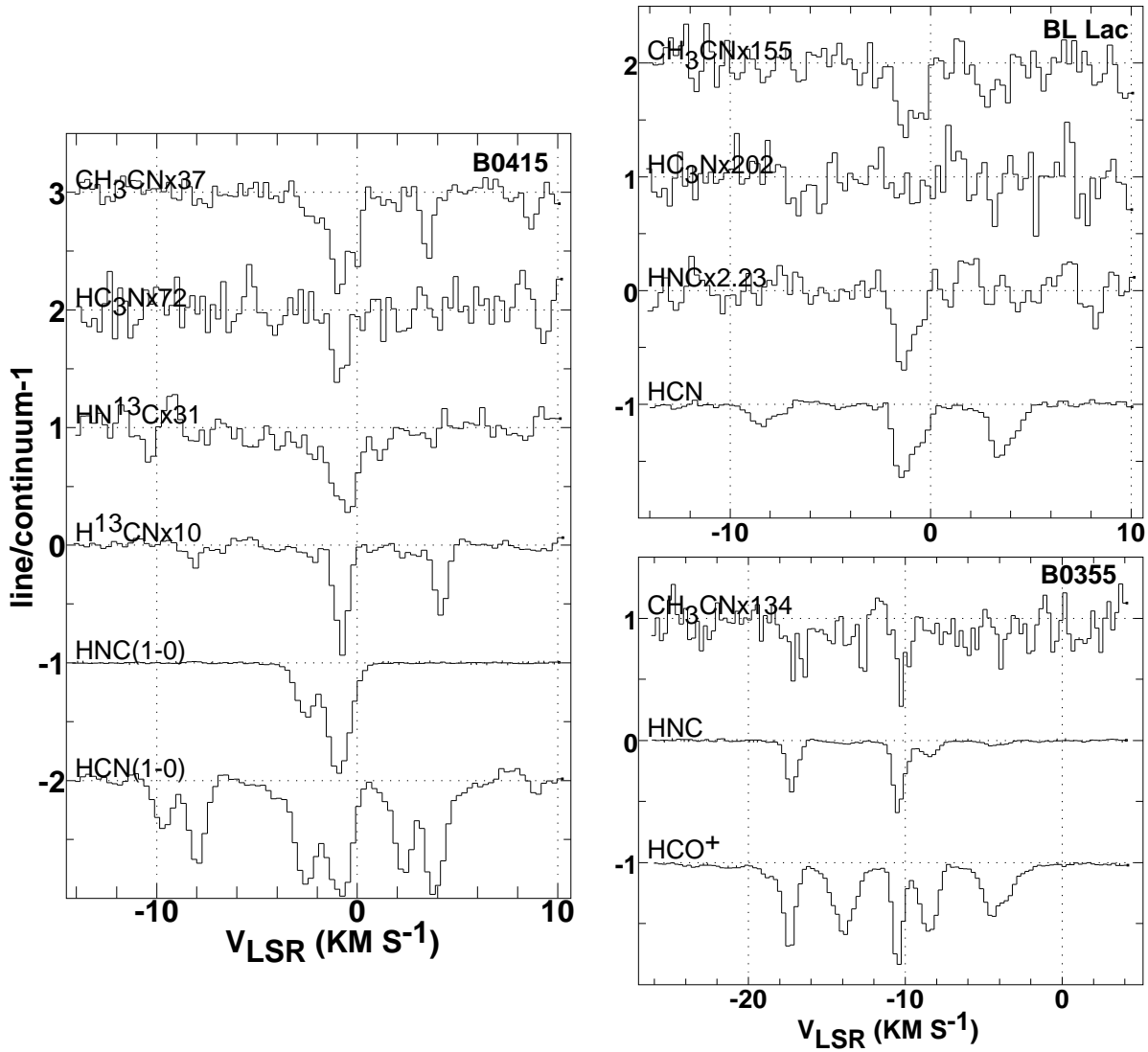
Figure 2 shows a source-by-source comparison of the newly-detected  $l$ - $C_3H$  with spectra of  $HCO^+$ , the species that shows the fullest extent of molecular absorption in our work.  $l$ - $C_3H$  is clearly a very ubiquitous species in diffuse molecular gas but with substantial variation in the ratio of the strength of the observed transition to that of  $J=1-0$   $HCO^+$ , as seen by comparing the individual features seen toward B0355. The expected variation of the optical depth-column density conversion factor for  $l$ - $C_3H$  is approximately 1 - 1.8 for densities in the number density range  $n(H_2) = 0 - 400 \text{ cm}^{-3}$  (Table 2).

Figure 3 compares spectra of the newly-detected CN-bearing species  $CH_3CN$  and  $HC_3N$  with those of previously-observed nitrogen-bearing species. The  $-17 \text{ km s}^{-1}$  and  $-11 \text{ km s}^{-1}$  components toward B0355+508 that are prominent in the CN-bearing species are just those that are weaker in  $l$ - $C_3H$  in Figures 1 and 2.

Table 3 gives integrated optical depths for the newly-observed species listed in Table 2 and Tables 4 - 6 give molecular column densities using the integrated optical depths in Table 3, calculated in the limiting case of no collisional excitation above the cosmic microwave background. For B0355+508 the results are listed separately for the kinematic components that are known to exist toward this source in  $HCO^+$ . For the other sources, results are shown integrated across the velocity range of the  $HCO^+$  profile.

### 2.4. Comparison with other milieu

The results for diffuse clouds from our work are compared with abundances for the same species determined in other environments in Tables 4 and 5 where detailed references are given, and in passing throughout the text. TMC-1 is the cyanopolyne peak in the Taurus Dark Cloud, the well-known Horsehead (HH) Nebula hosts a PDR and dense core that are distinguished in the tables. B1b is a complex dark



**Figure 3.** Line profiles of nitrogen-bearing species toward B0415+379, B2200+420 and B0355+508, vertically displaced and scaled as indicated. The CH<sub>3</sub>N and CH<sub>3</sub>CN profiles are new from this work. The HCN spectrum is not included for B0355 owing to the complexity of the kinematic structure.

cloud core that has higher density and 3-10 times higher column density than TMC-1. Abundances in the Orion Bar are as noted in the references in the tables.

### 3. THE ABUNDANCES OF SMALL HYDROCARBONS

We previously showed that *c*-C<sub>3</sub>H was ubiquitous in local diffuse molecular gas (Liszt et al. 2014b) and the present work extends this statement to the linear variant *l*-C<sub>3</sub>H. By contrast, C<sub>4</sub>H is not detected. Based on the accumulated data shown in Table 4 and previous results for C<sub>4</sub>H (Liszt et al. 2012) we summarize the chemistry of small hydrocarbons as follows:

- C<sub>2</sub>H is generally the most abundant hydrocarbon. N(C<sub>2</sub>H)  $\gtrsim$  N(CH) in diffuse molecular gas and dark cloud gas.
- The fractional abundance of C<sub>2</sub>H is the same in dif-

fuse molecular gas ( $4 \pm 2 \times 10^{-8}$ ) and toward TMC-1 ( $3 - 5 \times 10^{-8}$ ), but much larger than toward B1b or the Horsehead environments ( $0.3 - 1.0 \times 10^{-8}$ ).

- Adding a third carbon beyond C<sub>2</sub>H to form C<sub>3</sub>H produces a drop of about a factor 100 in column density in all environments. The drop is larger in diffuse molecular gas (N(C<sub>2</sub>H)/N(C<sub>3</sub>H)  $\approx$  200) than in dark cloud gas or the Horsehead (N(C<sub>2</sub>H)/N(C<sub>3</sub>H)  $\approx$  30–70) if *c*-C<sub>3</sub>H is considered. However, the drop is more nearly equal to 100 in all environments if the comparison is based on *l*-C<sub>3</sub>H.
- The cyclic/linear ratio N(*c*-C<sub>3</sub>H)/N(*l*-C<sub>3</sub>H)  $\approx$  0.5 in diffuse molecular gas, comparable to what is observed in the circumstellar envelope around the evolved star IRC+10216 (0.4, see Agúndez et al. (2008)), but very different from the values N(*c*-C<sub>3</sub>H)/N(*l*-C<sub>3</sub>H)  $\approx$  3–10

in the other environments shown in Table 4.

- The linear variant is much less abundant relative to cyclic in  $C_3H_2$  than in  $C_3H$ . The linear/cyclic ratio  $N(l-C_3H_2)/N(c-C_3H_2) \ll 1$  in diffuse molecular gas and the Horsehead environments, 1/40 - 1/15, and slightly larger, 1/7-1/6, in dark cloud gas.
- Abundance does not fall uniformly with complexity,  $C_2H$  being at least as abundant as  $CH$ , and  $c-C_3H_2$  being more abundant than  $c-C_3H$ .  $N(l-C_3H)/N(l-C_3H_2) \approx 1 - 3$  in all environments, and slightly larger in diffuse molecular gas than otherwise.  $N(c-C_3H)/N(c-C_3H_2) \approx 1/10$  in diffuse molecular gas, only slightly less than in dark cloud gas (1/6-1/7). The Horsehead environments have ratios nearer unity,  $N(c-C_3H)/N(c-C_3H_2) \approx 1/2$
- The ratios  $N(l-C_3H)/N(c-C_3H_2) \approx 0.1 - 0.2$  observed here (Table 4) are quite comparable to those observed toward Sgr B2 by Corby et al. (2017) in gas of indeterminate  $E_{B-V}$ .
- $N(C_4H)/N(C_2H) \ll 1$  for diffuse molecular gas, smaller than toward TMC-1 where  $N(C_4H)/N(C_2H) \approx 0.5$  as we have summarized in Table 4 albeit with large uncertainty in  $N(C_4H)$  for TMC-1, see also Liszt et al. (2012). Our measurements of  $N(C_4H)$  are insufficiently sensitive to make worthwhile comparisons with  $C_3H$ .

The situation is summarized in Figure 5. At left, the molecular column densities are plotted against the far IR dust emission-derived optical reddening equivalents given in Table 1 (Schlegel et al. 1998) and only the total column density toward B0355 can be used; at right the individual kinematic components have been measured for several but not all molecules toward B0355. Also shown in this Figure are values of  $N(C_3)$  and  $N(C_2)$ , using the  $C_3$  column densities of Ádámkóvics et al. (2003) and Oka et al. (2003)<sup>1</sup>, the  $C_2$  column densities cited in either paper and the  $CH$  column densities given by Oka et al. (2003). Inclusion of the results for  $C_2$  and  $C_3$  was motivated by the central role attributed to  $C_3$  in small-hydrocarbon formation in dark clouds by Loison et al. (2017), see their Figure 3. Ironically,  $N(C_3)$  is not observable in dark clouds so Loison et al. (2017) did not tabulate calculated values of  $N(C_3)$  from their models. Triatomic carbon is observed at THz frequencies in the envelopes and cores of star-forming regions like DR21(OH) with a fractional abundance  $X(C_3) \approx 0.6 - 3.0 \times 10^{-9}$  (Mookerjee et al. 2012), comparable to what is shown here in Figure 5<sup>2</sup>. CO aside,  $C_2$  is

<sup>1</sup> The  $C_3$  column densities in common between these references only agree to within a factor two or so

<sup>2</sup> Abundances of  $C_2H$  and  $c-C_3H_2$  are also comparable.

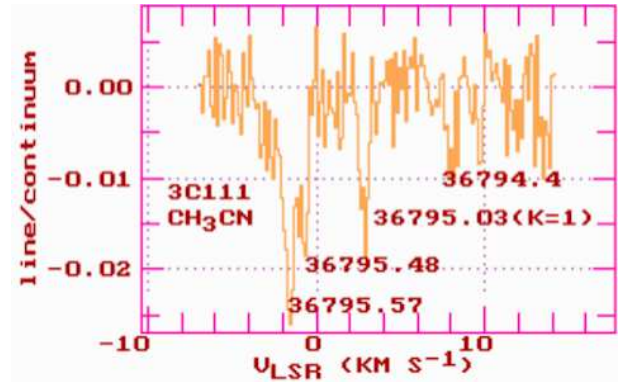


Figure 4. Closeup of  $CH_3CN$   $K=0$  and  $K=1$  lines (Table 1) toward B0415 at  $0.127 \text{ km s}^{-1}$  spectral resolution.

the most abundant carbon-bearing molecule in diffuse molecular gas, 2-3 times more abundant than either  $CH$  or  $C_2H$ . The factor 40 drop in abundance between  $C_2$  and  $C_3$  is twice as large as that between  $C_2H$  and  $c-C_3H_2$ .

Loison et al. (2017) consider in detail the formation of the isomers of the molecular ions that recombine to form  $C_3H$  and  $C_3H_2$  along with those of their recombination products, and they took into account the subsequent linear  $\rightarrow$  cyclic isomerization arising from reaction with free atomic hydrogen. They conclude that the comparatively small  $c-C_3H/l-C_3H$  ratio ( $\approx 5$ ) in dark clouds is created during initial formation, either via the reaction of  $C + C_2H_2$  or by dissociative recombination, while the much larger values 30-100 seen in  $C_3H_2$  arise after formation of  $l-C_3H_2$  through linear  $\rightarrow$  cyclic isomerization in reaction with atomic hydrogen.

The  $c-C_3H_2/l-C_3H_2$  ratio in dark clouds decreases with increasing density, which is understood in terms of the smaller atomic hydrogen fraction in denser gas. While this may occur, the much larger atomic hydrogen fraction in diffuse and translucent gas does not lead to yet-larger  $c-C_3H_2/l-C_3H_2$  ratios in our observations, which show quite comparable values to those seen in dark clouds. The inverted ratios  $c-C_3H/l-C_3H \approx 0.5$  in our work have no precedent in dark clouds.

#### 4. THE ABUNDANCE OF POLYINES AND CN-BEARING SPECIES

- CN itself is the most abundant CN-bearing molecule.  $N(CN)/N(H_2) = 3 \times 10^{-8}$  in diffuse molecular gas and toward TMC-1, or  $N(CN)/N(H_2) = 1 \times 10^{-8}$  toward B1b.
- $N(CN)/N(HCN) \approx 7$  in diffuse molecular gas vs. 1-1.5 in dark cloud gas
- $N(HCN)/N(HNC) \approx 3-6$  in diffuse molecular gas vs. 1 in dark cloud gas, a sign of warmer chemistry in diffuse gas.
- $N(HC_3N)/N(HCN) \leq 0.4$  in diffuse molecular gas comparable to B1b but much less than TMC-1 where  $N(HC_3N)/N(HCN) \approx 60$ .

- $N(\text{CH}_3\text{CN})/N(\text{HCN}) \approx 0.015$  in diffuse molecular gas comparable to TMC-1 (0.02) but much greater than B1b (0.002).
- $N(\text{CH}_3\text{CN})/N(\text{HC}_3\text{N}) = 4$  toward B0415, much larger than in dark clouds (1/20 - 1/30), so CH<sub>3</sub>CN is enhanced but not by as much as in the Horsehead PDR.
- The large values  $N(\text{CH}_2\text{CN})/N(\text{CH}_3\text{CN}) \approx 10$  in dark clouds are not seen in diffuse molecular gas.
- There is no fiducial value for  $N(\text{CH}_3\text{NC})/N(\text{CH}_3\text{CN})$  in dark cloud gas but the best upper limits  $N(\text{CH}_3\text{NC})/N(\text{CH}_3\text{CN}) < 0.15 - 0.3$  in diffuse molecular gas are comparable to the abundance ratio  $N(\text{CH}_3\text{NC})/N(\text{CH}_3\text{CN}) = 0.15$  seen toward the Horsehead PDR.

The overall situation is summarized in Figure 6 where the optical absorption measurements of  $N(\text{CN})$  and  $N(\text{C}_2)$  cited by [Oka et al. \(2003\)](#) are also included. CN itself is the most abundant CN-bearing molecule, with column densities about 1/3 - 1/2 those of C<sub>2</sub>, or comparable to those of CH, at larger  $E_{B-V}$  or  $N(\text{CH})$ . The main result is of course the surprising ubiquity of CH<sub>3</sub>CN in diffuse molecular gas, with  $X(\text{CH}_3\text{CN}) = N(\text{CH}_3\text{CN})/N(\text{H}_2) \approx 0.85 \times 10^{-10}$ . That said, there is another surprise in Figure 6: optical CN absorption line data at intermediate  $E_{B-V}$  or  $N(\text{CH})$  where  $N(\text{CN})$  measured in optical absorption is much smaller than  $N(\text{CN})$  measured in the radio at the same  $E_{B-V}$ . In mm-wave absorption, CN, HCN and HNC appear in nearly fixed proportions ([Liszt & Lucas 2001](#); [Ando et al. 2016](#)), with  $N(\text{CN})/N(\text{HCN}) = 7 \pm 1$ . Smaller CN abundances measured in absorption toward early-type stars would suggest photodissociation of CN, especially, as the likely cause. Lamentably, the abilities of optical/UV absorption spectroscopy have not yet allowed detection of species such as HCN in the absorption spectra of stars occulted by diffuse clouds. The optical/UV spectra of HCN and HNC have recently been calculated by [Aguado et al. \(2017\)](#) as part of a computation of the photodissociation rates of both species, showing that the photodissociation rate of HNC is 2.2 times greater. This could account in part for the higher  $N(\text{HCN})/N(\text{HNC})$  ratios in diffuse clouds, compared to TMC-1 (see Figure 6 and Table 5).

## 5. OXYGEN-BEARING SPECIES

Limits on the column densities of isocyanic acid (HNCO), formic acid (HCOOH; found on Earth in ants, bees and nettle plants according to its discoverers [Zuckerman et al. \(1971\)](#)) in the interstellar medium (ISM) and protonated formaldehyde (H<sub>2</sub>COH<sup>+</sup>) are given in Table 6. HNCO and HCOOH were observed in their lowest transitions, leading to rather large uncertainties in their column densities as noted in Table 1. HNCO can only be said to be less abundant in diffuse molecular gas than in TMC-1 if the excitation is weak

in the diffuse molecular gas. There is no fiducial value of the column density of protonated formaldehyde (H<sub>2</sub>COH<sup>+</sup>) for TMC-1.

## 6. CH<sub>2</sub>CN<sup>-</sup> AS A POSSIBLE DIB CARRIER

[Cordiner & Sarre \(2007\)](#) proposed the para-ladder rotational transitions of the anion CH<sub>2</sub>CN<sup>-</sup> as the carrier of a diffuse interstellar band (DIB) at  $\lambda 803.7\text{nm}$ . It is this ladder whose lowest rotational transition was observed here in the neutral version of the molecule, CH<sub>2</sub>CN. The neutral and its anion have the same symmetry properties, similar rotational structure and roughly comparable permanent dipole moments (3.6 vs. 1.2 Debye, respectively) ([Majumdar et al. 2014](#)) so that arguments used in the discussion of the required abundance of the anion should also be used when comparing its column density with that of the neutral observed here. As shown in Table 3, the ratios  $N(\text{CH}_2\text{CN})/N(\text{CN})$  and  $N(\text{CH}_2\text{CN})/N(\text{HCN})$  are at least about one order of magnitude smaller in diffuse molecular gas than in dark cloud gas toward TMC-1.

Using Herbig's unpublished data [Cordiner & Sarre \(2007\)](#) determined equivalent widths toward eight stars having reddening  $E_{B-V} = 1 - 1.4$  mag, quite comparable to those toward B0355 and B0415 in this work. The results are  $\langle W_\lambda/E_{B-V} \rangle = 0.00220 \pm 0.00064$  nm/mag, or  $\langle N(p\text{-CH}_2\text{CN}^-)/E_{B-V} \rangle = 4.025 \times 10^{10}/f$  cm<sup>-2</sup>/mag where  $f$  is the oscillator strength of the  $\lambda 803.7\text{nm}$  transition. [Cordiner & Sarre \(2007\)](#) hypothesized  $f=0.5$ , leading to an implied column density  $N(p\text{-CH}_2\text{CN}^-) = 1.2 - 1.3 \times 10^{11}$  cm<sup>-2</sup> toward B0355 and B0415. The upper limits we deduce for  $N(p\text{-CH}_2\text{CN})$  toward these sources are somewhat above this,  $N(p\text{-CH}_2\text{CN}) < 2.5 \times 10^{11}$  cm<sup>-2</sup> before applying a correction for rotational excitation above that provided by radiative equilibrium with the cosmic microwave background, which is in the range 1-3.

[Cordiner & Sarre \(2007\)](#) showed that two strong spectral features corresponding to absorption out of the ortho-ladder  $K=1$  levels were absent in the optical spectrum, implying that all of the CH<sub>2</sub>CN<sup>-</sup> resided in the para rotational ladder<sup>3</sup>. To explain this, [Cordiner & Sarre \(2007\)](#) argued that the ortho/para ratio was small because weak collisional excitation in the diffuse molecular ISM would leave all molecules in the lowest possible states, in radiative equilibrium with the cosmic microwave background in all facets of the excitation. Our calculations show that this is a poor assumption for the para-ladder given the large electron fraction in diffuse molecular gas and the large permanent dipole moments of the species in question, but the optical profiles that were integrated to give the equivalent widths naturally include the poorly-resolved rotational sub-structure even if [Cordiner & Sarre \(2007\)](#) did not consider it to be

<sup>3</sup> In fact this could easily be taken to disqualify CH<sub>2</sub>CN<sup>-</sup> as the carrier.

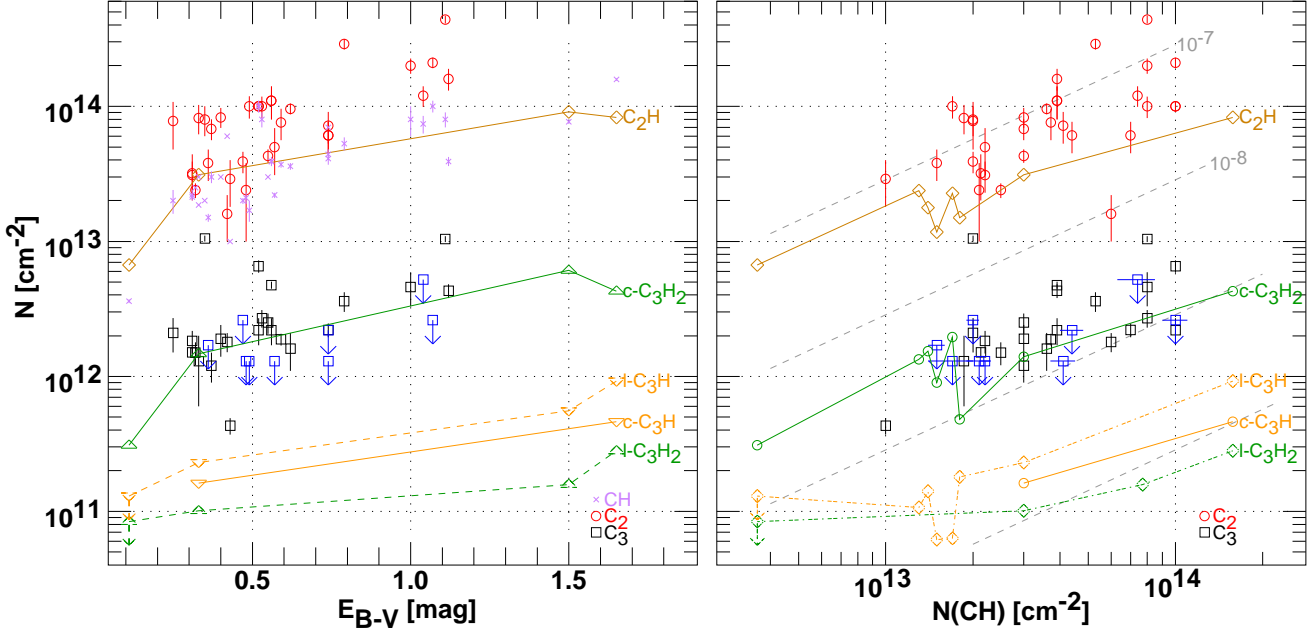


**Figure 5.** Column densities of  $C_3$ ,  $C_2$  (Ádámkóvics et al. 2003; Oka et al. 2003),  $CH$  (Oka et al. 2003) and small hydrocarbons (Table 4). Shown at left are column densities plotted against the IR dust emission-derived optical reddening equivalents (Table 1) for the radio data, or using the stellar reddening for the optical  $C_2$ ,  $C_3$  and  $CH$  data. At right, column densities are plotted against  $N(CH)$  using the individual component column densities for the radio data where possible and using  $N(CH)$  cited by Oka et al. (2003) for the sightlines observed in optical absorption. Dashed gray lines at right show fractional abundance with respect to  $H_2$  assuming  $N(CH)/N(H_2) = 3.5 \times 10^{-8}$ .

present. The point is that we are obliged to compare the required column density of  $p\text{-CH}_2\text{CN}^-$  with upper limits for  $p\text{-N}(\text{CH}_2\text{CN})$  that are fully corrected for rotational excitation within the para-rotation ladder even if they weaken our conclusions.

Our limits on  $N(p\text{-CH}_2\text{CN})$  are above the required column density of the anion by a factor of a few, 2-6. Under normal circumstances, the large neutral/anion column density ratios  $> 200$  found for other species (Satta et al. 2015) would exclude  $\text{CH}_2\text{CN}^-$  as a possible carrier of the DIB at  $\lambda 803.7\text{nm}$ . However, Cordiner & Sarre (2007) argued, on the basis of unpublished work by E. Herbst and T. Millar, that the neutral/anion ratio would be exceptionally small,  $N(\text{CH}_2\text{CN})/N(\text{CH}_2\text{CN}^-) \approx 1$ .

Indeed, small ratios  $N(\text{CH}_2\text{CN})/N(\text{CH}_2\text{CN}^-) = 0.25 - 0.6$  were subsequently calculated by Majumdar et al. (2014) who tracked the time evolution of a comprehensive chemical network over a wide range of  $A_V$  and  $n(\text{H})$ . However, the models of Majumdar et al. (2014) also predict  $N(\text{CH}_2\text{CN}^-) = 3.5 \times 10^7 \text{ cm}^{-2}$  and  $N(\text{CH}_3\text{CN}) = 1.4 \times 10^5 \text{ cm}^{-2}$  at  $A_V = 1 \text{ mag}$  and  $n(\text{H}) = 350 \text{ cm}^{-3}$ . These are some 4 orders of magnitude below the required column density of  $N(\text{CH}_2\text{CN}^-)$  but also more than five orders of magnitude below our newly-observed column density of  $\text{CH}_3\text{CN}$  toward B2200+420 (BL Lac) at  $A_V = 1 \text{ mag}$  in Table 5. Clearly, the chemistry of  $\text{CH}_2\text{CN}^-$ , and other important anions and molecules possibly linked to DIBs in diffuse molecular gas, must be revisited.

To summarize, our observational upper limit suffices to show that the ratios  $N(\text{CH}_2\text{CN})/N(\text{CN})$  and

$N(\text{CH}_2\text{CN})/N(\text{HCN})$  are at least about one order of magnitude smaller in diffuse molecular gas than toward TMC-1. But if it is accepted that the neutral/anion ratio is so much smaller for  $\text{CH}_2\text{CN}$  than for other species,  $\text{CH}_2\text{CN}^-$  might remain a viable carrier of the DIB at  $\lambda 803.7\text{nm}$ .

## 7. COMS IN DIFFUSE CLOUDS?

Claims for the presence of various oxygen and nitrogen bearing complex organic molecules (COMS) in diffuse clouds have recently been made on the basis of ALMA observations toward Sgr B2 (Thiel et al. 2017). Some of the column densities derived in that work are shown in Table 7, where we copied results for the three galactic center clouds appearing near 0-velocity (their Table 1) and for the cloud at  $+27 \text{ km s}^{-1}$  assumed to lie in the Scutum arm (their Table 2). For comparison we show results for TMC-1 ( $A_V = 10\text{-}20 \text{ mag}$ ) and B2200 ( $A_V = 1 \text{ mag}$ ), largely as shown in our Tables 5 and 6. For TMC-1 and B2200 we take  $N(\text{H}^{13}\text{CO}^+) = N(\text{HCO}^+)/62$ , the result obtained for local gas (Lucas & Liszt 1998). The results for  $N(\text{CH}_3\text{OH})$  are taken from Liszt et al. (2008) for B2200 and from Ohishi et al. (1992) and Gratier et al. (2016) for TMC-1.

$\text{HCO}^+$  and  $c\text{-C}_3\text{H}_2$  are often used as  $\text{H}_2$  tracers, for instance with  $X(\text{HCO}^+) = N(\text{HCO}^+)/N(\text{H}_2) = 3 \times 10^{-9}$  here, or  $X(c\text{-C}_3\text{H}_2) = 2.5 \times 10^{-9}$  in the work of Riquelme et al. (2017). As shown in Table 7, the column densities of  $\text{HCO}^+$  in the features described as diffuse clouds toward Sgr B2 range from 15 to 200 times larger than toward B2200 and are comparable to or even larger than what is observed in



TMC-1<sup>4</sup>. The *c*-C<sub>3</sub>H<sub>2</sub> column densities seen toward Sgr B2 range up to 12 times that seen toward B2200. Clouds with such comparatively high column densities of the tracers of H<sub>2</sub> cannot also have  $A_V \lesssim 1$  mag, the usual meaning of the term “diffuse” (Snow & McCall 2006).

The column densities toward Sgr B2 are 3-20 times larger than toward TMC-1 for CH<sub>3</sub>OH, 3-5 times larger than TMC-1 for CH<sub>3</sub>CN, and as much as 5 times larger than TMC-1 for HC<sub>3</sub>N. They are all several hundred times larger than seen toward B2200. COMS may have been observed toward Sgr B2, but the nature of the host gas remains to be determined.

## 8. SUMMARY AND DISCUSSION

This work completes several major aspects of a long work program to catalog and systematize the molecular inventory of diffuse molecular gas observed in absorption at radio wavelengths near the Sun and in the wider Galaxy outside the central molecular zone, extending it beyond the very limited complement of mostly-diatomic molecules seen at UV through NIR wavelengths. The case for comparability of the diffuse molecular gas observed in the radio and UV through NIR domains was made in our recent discussions of the suitability of small polar species as carriers of DIBs (Liszt et al. 2012, 2014a) and will not be repeated here, keeping the focus on the observable chemistry of the detected hydrocarbons and CN-bearing species. The oxygen-bearing family of molecules observed at radio wavelengths (OH, CO, HCO, HCO<sup>+</sup>, HOC<sup>+</sup>, H<sub>2</sub>CO and CH<sub>3</sub>OH) will be discussed in a forthcoming work that includes recent ALMA observations of HOC<sup>+</sup> and comparisons with existing HERSCHEL observations of H<sub>2</sub>O.

The systematics of the small hydrocarbons and CN-bearing species are comprehensively outlined in Sections 3 and 4, respectively. The most abundant species in each family, CH or C<sub>2</sub>H and CN, have relative abundances with respect to H<sub>2</sub> that are about equal to each other and the same in diffuse molecular gas and TMC-1,  $X(\text{C}_2\text{H}) = N(\text{C}_2\text{H})/N(\text{H}_2) = 4 \times 10^{-8}$  and  $X(\text{CN}) = 3 \times 10^{-8}$  at higher  $E_{B-V}$  or  $N(\text{H}_2)$ . However, the most abundant carbon-bearing molecule overall among those considered here (ie, neglecting CO), is C<sub>2</sub> with  $X(\text{C}_2) = 8 \times 10^{-8}$ , 2-3 times more abundant than CH, C<sub>2</sub>H or CN. The factor 40 drop in abundance between C<sub>2</sub> and C<sub>3</sub> is twice as large as that between C<sub>2</sub>H and *c*-C<sub>3</sub>H<sub>2</sub>.

In this work we showed that *l*-C<sub>3</sub>H and CH<sub>3</sub>CN are ubiquitous in local diffuse molecular gas and the ratio of CH<sub>3</sub>CN to HCN is the same as in TMC-1,  $N(\text{CH}_3\text{CN})/N(\text{HCN}) \approx 0.02$ . The relative abundance of *c*-C<sub>3</sub>H is about the same in diffuse molecular gas as in TMC-1 or dark clouds generally Liszt et al. (2014b) but the linear variant is enhanced in dif-

fuse molecular gas:  $N(\text{c-C}_3\text{H})/N(\text{l-C}_3\text{H}) \approx 0.5$  in diffuse molecular gas, vs 4-10 in the other environments considered in Tables 3-4. The linear variant is much more abundant relative to cyclic in C<sub>3</sub>H than in C<sub>3</sub>H<sub>2</sub> in all environments.

The *c*-C<sub>3</sub>H<sub>2</sub>/*l*-C<sub>3</sub>H<sub>2</sub> ratio in dark clouds decreases with increasing density, which is understood in terms of the smaller atomic hydrogen fraction in denser gas. The much larger atomic hydrogen fraction in diffuse and translucent gas does not lead to yet-larger *c*-C<sub>3</sub>H<sub>2</sub>/*l*-C<sub>3</sub>H<sub>2</sub> ratios in our observations, which show quite comparable values to those seen in dark clouds. The inverted ratios *c*-C<sub>3</sub>H/*l*-C<sub>3</sub>H  $\approx 0.5$  in our work have no precedent in dark clouds.

In Section 6 we discussed the suitability of CH<sub>2</sub>CN<sup>-</sup> as a DIB-carrier (Cordiner & Sarre 2007) based on the limits we were able to set on  $N(\text{CH}_2\text{CN})$ . For CH<sub>2</sub>CN to be a viable candidate DIB-carrier, the neutral/anion ratio would have to be small, no more than 2-6. Neutral/anion ratios for observed species are typically 200:1 or larger (Satta et al. 2015).

In Section 7 we compared our results with those of Thiel et al. (2017) for three low-velocity clouds and another in the Scutum Arm observed in absorption toward Sgr B2: these observations are the basis of claims for the existence of complex organic molecules (COMS) in diffuse clouds. We noted that column densities of H<sub>2</sub>-tracers such as HCO<sup>+</sup> were one - two orders of magnitude higher in that work than those we associate with clouds at  $A_V \lesssim 1$  mag locally, and in some cases even larger than those seen in TMC-1. Claims for the presence of COMS in diffuse clouds, material at  $A_V \lesssim 1$  mag, must be carefully assessed.

Describing the molecular inventory of diffuse molecular gas is still a work in progress: outstanding undetected hydrocarbons with three carbon atoms include CH<sub>3</sub>C<sub>2</sub>H and the recently-introduced *t*-C<sub>3</sub>H<sub>2</sub> (Loison et al. 2017) whose microwave spectrum is unknown. *t*-C<sub>3</sub>H<sub>2</sub> could be a common host of unidentified lines given the ubiquity of the other isomers of C<sub>3</sub>H<sub>2</sub> in a wide range of astrophysical environments.

Understanding the observed abundance of even some quite small species (CH<sup>+</sup>, HCO<sup>+</sup>) in diffuse molecular gas requires the addition of new physics into the chemical modelling, as embodied in the work of Godard et al. (2014) and Valdivia et al. (2017). It has further been suggested that the small hydrocarbons observed here should originate in a top-down chemistry after the breakup of much larger species (Guzmán et al. 2015). Observations of polycyclic aromatic hydrocarbons with the James Webb Space Telescope may soon test this idea.

The National Radio Astronomy Observatory is operated by Associated Universities, Inc. under a contract with the National Science Foundation. HL, MG and JP were partially funded by the grant ANR-09-BLAN-0231-01 from the French *Agence Nationale de la Recherche* as part of the SCHISM project (<http://schism.ens.fr/>) during the early

<sup>4</sup> The very largest disparities might be explained in small part by a smaller  $N(\text{HCO}^+)/N(\text{H}^{13}\text{CO}^+)$  ratio if the material near 0-velocity toward Sgr B2 is actually in the central molecular zone.

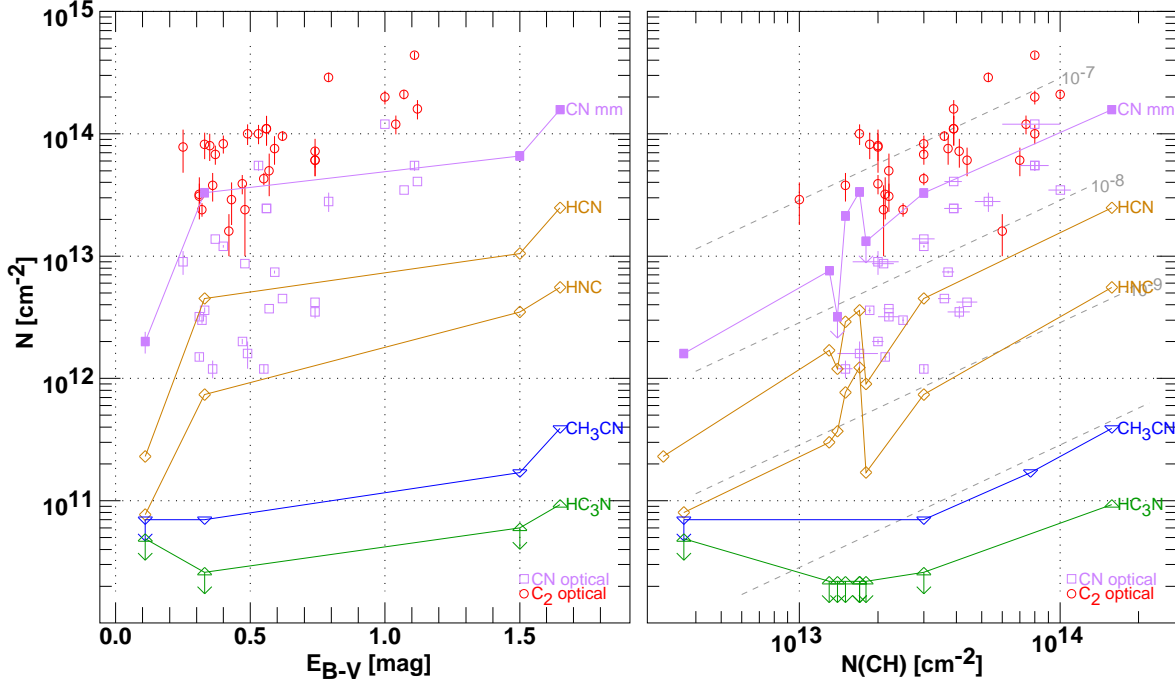


**Figure 6.** Column densities of  $C_2$  (Ádámkóvics et al. 2003; Oka et al. 2003), CH (Oka et al. 2003) and CN-bearing species (Table 5). Shown at left are column densities plotted against the IR dust emission-derived optical reddening equivalents (Table 1) for the radio data, or using the stellar reddening for the optical  $C_2$  and CN data. At right, column densities are plotted against  $N(CH)$  using the individual component column densities for the radio data where possible and using  $N(CH)$  cited by Oka et al. (2003) for the sightlines observed in optical absorption. Dashed gray lines at right show fractional abundance with respect to  $H_2$  assuming  $N(CH)/N(H_2) = 3.5 \times 10^{-8}$ .

**Table 1.** Continuum target and sightline properties

Target	aka	l °	b °	$E_{B-V}^a$ mag	flux <sup>b</sup> %
B0355+508	NRAO150	150.38	-1.60	1.50	28,29
B0415+379	3C111	161.67	-8.82	1.65	8,10
B2200+420	BL Lac	92.59	-10.44	0.33	28,31
B2251+158	3C454.3	86.11	-38.18	0.11	16,21

<sup>a</sup>from Schlegel et al. (1998)

<sup>b</sup> entries are 21 GHz and 36 GHz fluxes as percentages of 3C84 ( $S_\nu \approx 16, 10$  Jy)

phases of this work. The work of MG and JP was supported by the CNRS program “Physique et Chimie du Milieu Interstellaire” (PCMI). The work of MG and JP was supported by the Programme National “Physique et Chimie du Milieu Interstellaire” (PCMI) of CNRS/INSU with INC/INP co-funded by CEA and CNES.

We thank the Alexandre Faure for providing excitation rates for  $CH_3CN$  and we thank the anonymous referee for a variety of remarks that led to improvements in the manuscript.

*Facility:* VLA

*Software:* DRAWSPEC (Liszt 1997), CASA (McMullin et al. 2007)

## APPENDIX

### A. ROTATIONAL EXCITATION

For the low-lying transitions of heavier species observed in this work, collisional excitation redistributes the rotational population out of the lowest states, increasing the numerical factors that should be used to convert observed optical depths to column density. Collisions with electrons greatly dominate the excitation in diffuse molecular gas where the CO abundance is small and  $C^+$  is the dominant carrier of carbon leading to an electron fraction  $n(e)/n(H) \gtrsim 1.4 \times 10^{-4}$  (Sofia et al. 2004). Excitation rates for collisions with He and  $H_2$  play a smaller role and have not been calculated for most of the species discussed here but we included  $H_2$  excitation of  $HC_3N$  (Faure et al. 2016) and excitation of  $CH_3CN$  by He and  $H_2$  (Faure, private communication). Electron excitation is considered here as in Liszt (2012), using separate closed-form approximations for molecular ions and neutrals.

The excitation rate coefficients and our excitation calculations are not hyperfine-resolved and are just recalculations of the rotational partition function. Results of the excitation calculations are illustrated in Figure A.1 for hydrocarbons and CN-bearing species and in Figure A.2 for the oxygen-bearing species. The normalization on the vertical axis is such that the integrated optical

**Table 2.** Species and transitions observed and column density-optical depth conversion factors at  $T_{\text{ex}}=T_{\text{CMB}}$ 

Species	ortho/para/other	transition	frequency MHz	$\log(A_{kj} \text{ s}^{-1})^a$	$N(X)/\int \tau dv^b$ $\text{cm}^{-2} (\text{km s}^{-1})^{-1}$	Correction <sup>e</sup>
<i>l</i> -C <sub>3</sub> H	<i>l</i> = <i>f</i>	J=3/2-1/2,Ω=1/2,F=2-1	32627.30	-5.89	$2.82 \times 10^{13}$	1-1.8
<i>l</i> -C <sub>3</sub> H	<i>l</i> = <i>e</i>	J=3/2-1/2,Ω=1/2,F=2-1	32660.65	-5.89	$2.82 \times 10^{13}$	1-1.8
HC <sub>3</sub> N <sup>c</sup>		J=4-3	36292.33	-5.49	$1.09 \times 10^{13}$	1-1.6
CH <sub>3</sub> CN	E	2(0)-1(0) F=3-2	36795.57	-5.45	$1.27 \times 10^{13}$	1-1.7
CH <sub>3</sub> CN	E	2(0)-1(0) F=2-1	36795.48	-5.57	$2.38 \times 10^{13}$	1-1.7
CH <sub>3</sub> CN	E	2(0)-1(0) F=1-0	36794.42	-5.70	$5.47 \times 10^{13}$	1-1.7
CH <sub>3</sub> CN	A	2(1)-1(1) F=1-0	36795.03	-5.57	$1.19 \times 10^{13}$	1-1.7
CH <sub>3</sub> NC	E	1(0)-0(0)	20105.75	-6.32	$1.07 \times 10^{13}$	1-4.5
CH <sub>2</sub> CN <sup>d</sup>	p	1 <sub>01</sub> - 0 <sub>00</sub>	20119.61	-6.41	$7.73 \times 10^{13}$	1-3.5
HNCO		1(0,1)-0(0,0) F=2-1	21981.46	-6.98	$6.39 \times 10^{13}$	1-6
HCOOH	t	1(0,1)-0(0,0)	22471.18	-7.07	$6.80 \times 10^{13}$	1-7
H <sub>2</sub> COH <sup>+</sup>		2(0,2)-1(1,1)	36299.95	-6.51	$5.61 \times 10^{13}$	1-1.6

<sup>a</sup> www.splatalogue.net<sup>b</sup> for the observed ortho or para version only, assuming rotational excitation in equilibrium with the cosmic microwave background<sup>c</sup> 96% of the integrated intensity is in an unresolved blend<sup>d</sup> J=3/2-1/2, F<sub>1</sub>=5/2-3/2, F=7/2-5/2. Spectroscopy from Irvine et al. (1988) and Ohishi & Kaifu (1998)<sup>e</sup> See Figures A1-A2**Table 3.** Integrated optical depths (EW) for newly-observed species <sup>a</sup>

Target	vel km s <sup>-1</sup>	EW m s <sup>-1</sup>	EW m s <sup>-1</sup>	EW m s <sup>-1</sup>	EW m s <sup>-1</sup>	EW m s <sup>-1</sup>	EW m s <sup>-1</sup>	EW m s <sup>-1</sup>	EW m s <sup>-1</sup>	EW m s <sup>-1</sup>
		<i>l</i> -C <sub>3</sub> H	HC <sub>3</sub> N	CH <sub>3</sub> CN <sup>b</sup>	CH <sub>3</sub> CN <sup>c</sup>	CH <sub>3</sub> NC	CH <sub>2</sub> CN	HNCO	HCOOH	H <sub>2</sub> COH <sup>+</sup>
B0355+508	-17	2.20(0.56)	< 2.0			< 1.71	< 1.90	< 2.10	< 2.21	< 3.63
	-14	6.40(0.64)								
	-10	2.22(0.48)								
	-8	3.56(0.56)								
	-4	5.00(0.70)								
	all	19.3(0.13)	< 5.5	23.0(3.0) <sup>d</sup>		< 4.47	< 3.24	< 4.86	< 4.80	< 7.98
B0415+379		32.8(1.75)	8.5(1.9)	42.4(3.2)	9.7(1.8)	< 4.16	< 3.15	< 4.62	< 4.62	< 9.30
B2200+420		8.16(0.4)	< 2.55	7.4(1.2)	2.3(0.6)	< 1.92	< 1.68	< 1.65	< 1.95	< 2.94
B2251+158		< 4.5	< 4.5	< 7.1		< 4.92	< 3.90			< 7.31

<sup>a</sup> all upper limits are 3σ<sup>b</sup> The sum of the three observed K=0 lines<sup>c</sup> K=1<sup>d</sup> K=0 and K=1 are not distinguishable, this is their sum

depth of the transition in question corresponds to a total column density  $N = 10^{11} \text{ cm}^{-2}$  (shown in each panel) but it is only the extent of the variation across the horizontal axis that matters. The default optical depth-column density conversion factor given in the next-to-last column of Table 2 corresponds to zero density at the left and the maximum correction corresponds to the amount by which the curves have fallen at  $n(\text{H}_2) = 400 \text{ cm}^{-3}$ . The very lowest-lying transitions are quite sensitive to density variations while those lying higher may be nearly unaffected. The excitation, being dominated by electrons, is only weakly sensitive to the kinetic temperature as shown in Figures A.1 and A.2 where the calculations have been carried out for kinetic temperatures of 20, 40 and 60 K: the different curves at these temperatures often overlap to the point that they are indistinguishable.

## REFERENCES

**Table 4.** Column densities for hydrocarbons

Target	$\nu$ km s <sup>-1</sup>	N(H <sub>2</sub> ) <sup>1</sup> 10 <sup>20</sup> cm <sup>-2</sup>	N(CH) <sup>2</sup> 10 <sup>13</sup> cm <sup>-2</sup>	N(C <sub>2</sub> H) <sup>a</sup> 10 <sup>13</sup> cm <sup>-2</sup>	N( <i>c</i> -C <sub>3</sub> H <sub>2</sub> ) <sup>b</sup> 10 <sup>12</sup> cm <sup>-2</sup>	N( <i>l</i> -C <sub>3</sub> H <sub>2</sub> ) <sup>c</sup> 10 <sup>11</sup> cm <sup>-2</sup>	N(C <sub>4</sub> H) <sup>m</sup> 10 <sup>13</sup> cm <sup>-2</sup>	N( <i>c</i> -C <sub>3</sub> H) <sup>d</sup> 10 <sup>11</sup> cm <sup>-2</sup>	N( <i>l</i> -C <sub>3</sub> H) 10 <sup>11</sup> cm <sup>-2</sup>
B0355	-17	4.3	1.5	1.17	0.90				0.62(0.16)
	-14	5.0	1.8	1.50	0.48				1.81(0.18)
	-10	4.8	1.7	2.27	1.96				0.63(0.14)
	-8	3.8	1.3	2.38	1.34				1.07(0.16)
	-4	4.0	1.4	1.78	1.54				1.41 (0.20)
	-all	22	7.7	9.10	6.11	1.58	<1		5.56(0.34)
B0415		45	15.8	8.29	4.28	2.81	< 2.3	4.63(0.18)	9.24(0.49)
B2200		8.7	3.0	3.11	1.47	1.01	< 0.4	1.62(0.05)	2.30(0.13)
B2251 <sup>e</sup>		1.0	0.36	0.67	0.31	< 0.84	< 0.3		< 1.3
TMC-1/10 <sup>f</sup>		10	2	5-10	10		2	6	5
TMC-1/10 <sup>g</sup>		''			2	0.6	0.3-9	18	6
TMC-1/10 <sup>h</sup>		''		6	12	2		10	1
TMC-1/10 <sup>i</sup>		''		2	6	2		10	1
consensus		10-20 <sup>f</sup>	2	5	6	1	2	9	2
B1b/10 <sup>j</sup>		≥ 60			2	0.6		6	1
HH PDR/10 <sup>k</sup>		19		1-2	0.5-0.8	0.5-1.5		2-7	0.6 - 1.8
HH core/10 <sup>k</sup>		32		< 1	0.3-0.4	0.1-0.3		0.8-2.3	0.1-0.4
Orion Bar/10 <sup>n</sup>		30		4	1.3	0.4	0.4	2	0.6

<sup>1</sup> N(H<sub>2</sub>) = N(HCO<sup>+</sup>)/3 × 10<sup>-9</sup> for sources observed in this work

<sup>2</sup> N(CH) = N(H<sub>2</sub>) × 3.5 × 10<sup>-8</sup> for sources observed in this work

<sup>a</sup> N(C<sub>2</sub>H) from [Lucas & Liszt \(2000\)](#)

<sup>b</sup> N(*c*-C<sub>3</sub>H<sub>2</sub>) = (4/3) × N(*o*-*c*-C<sub>3</sub>H<sub>2</sub>) from [Liszt et al. \(2012\)](#)

<sup>c</sup> N(*l*-C<sub>3</sub>H<sub>2</sub>) = 4 × N(*p*-*l*-C<sub>3</sub>H<sub>2</sub>) from [Liszt et al. \(2012\)](#)

<sup>d</sup> N(*c*-C<sub>3</sub>H) from [Liszt et al. \(2014b\)](#)

<sup>e</sup> upper limits are 3σ

<sup>f</sup> [Ohishi et al. \(1992\)](#) whose tables must be interpreted with N(H<sub>2</sub>) = 10<sup>22</sup> cm<sup>-2</sup>

<sup>g</sup> [Gratier et al. \(2016\)](#)

<sup>h</sup> [Loison et al. \(2017\)](#) except C<sub>2</sub>H from [Sakai et al. \(2010\)](#)

<sup>i</sup> [Fossé et al. \(2001\)](#)

<sup>j</sup> [Loison et al. \(2017\)](#) and [Daniel et al. \(2013\)](#)

<sup>k</sup> Horsehead (HH) nebula values from [Guzmán et al. \(2015\)](#)

<sup>l</sup> N(H<sub>2</sub>) ≥ 2 × 10<sup>22</sup> cm<sup>-2</sup> beam-averaged on 1' scales is given by [Fehér et al. \(2016\)](#)

<sup>m</sup> Results for C<sub>4</sub>H from [Liszt et al. \(2012\)](#)

<sup>n</sup> [Cuadrado et al. \(2015\)](#), Table 6

Agúndez, M., Cernicharo, J., Pardo, J. R., et al. 2008, *Astrophys. Space Sci.*, 313, 229

Ando, R., Kohno, K., Tamura, Y., et al. 2016, *Publ. Astron. Soc. Jpn.*, 68, 6

Corby, J., McGuire, B., Herbst, E., & Remijan, A. 2017, *ArXiv e-prints*, arXiv:1708.03432

Cordiner, M. A., & Sarre, P. J. 2007, *A&A*, 472, 537

Cuadrado, S., Goicoechea, J. R., Cernicharo, J., et al. 2017, *A&A*, 603, A124

Cuadrado, S., Goicoechea, J. R., Pilleri, P., et al. 2015, *A&A*, 575, A82

Daniel, F., Gerin, M., Roueff, E., et al. 2013, *A&A*, 560, A3

Faure, A., Lique, F., & Wiesenfeld, L. 2016, *Mon. Not. R. Astron. Soc.*, 460, 2103

Fehér, O., Tóth, L. V., Ward-Thompson, D., et al. 2016, *A&A*, 590, A75

Fossé, D., Cernicharo, J., Gerin, M., & Cox, P. 2001, *ApJ*, 552, 168

Gerin, M., Neufeld, D. A., & Goicoechea, J. R. 2016, *Ann. Rev. Astrophys. Astron.*, 54, 181

Glassgold, A. E., & Langer, W. D. 1975, *ApJ*, 197, 347

Godard, B., Falgarone, E., & Pineau des Forêts, G. 2014, *A&A*, 570, A27

Gratier, P., Majumdar, L., Ohishi, M., et al. 2016, *Astrophys. J., Suppl. Ser.*, 225, 25

Gratier, P., Pety, J., Guzmán, V., et al. 2013, *A&A*, 557, A101

Guzmán, V. V., Pety, J., Goicoechea, J. R., et al. 2015, *ApJ*, 800, L33

Irvine, W. M., Friberg, P., Hjalmarsen, A., et al. 1988, *ApJ*, 334, L107

Liszt, H., & Lucas, R. 2001, *A&A*, 370, 576

Liszt, H., Lucas, R., & Pety, J. 2006, *A&A*, 448, 253

Liszt, H., Lucas, R., Pety, J., & Gerin, M. 2014a, in *IAU Symposium, Vol. 297, The Diffuse Interstellar Bands*, ed. J. Cami & N. L. J. Cox, 163–172

Liszt, H., Sonnentrucker, P., Cordiner, M., & Gerin, M. 2012, *ApJ*, 753, L28

Liszt, H. S. 1997, in *Astronomical Society of the Pacific Conference Series, Vol. 125, Astronomical Data Analysis Software and Systems VI*, ed. G. Hunt & H. Payne, 3

Liszt, H. S. 2007, *A&A*, 476, 291

— 2012, *A&A*, 538, A27

— 2017, *ApJ*, 835, 138

Liszt, H. S., & Gerin, M. 2016, *A&A*, 585, A80

Liszt, H. S., Guzmán, V. V., Pety, J., et al. 2015, *A&A*, 579, A12

Liszt, H. S., & Lucas, R. 1996, *A&A*, 314, 917

Liszt, H. S., & Pety, J. 2016, *ApJ*, 823, 124

Liszt, H. S., Pety, J., Gerin, M., & Lucas, R. 2014b, *A&A*, 564, A64

**Table 5.** Column densities for CN-family molecules<sup>a</sup>

Target	$\nu$ km s <sup>-1</sup>	N(H <sub>2</sub> ) 10 <sup>20</sup> cm <sup>-2</sup>	N(CN) <sup>b</sup> 10 <sup>13</sup> cm <sup>-2</sup>	N(HCN) <sup>b</sup> 10 <sup>13</sup> cm <sup>-2</sup>	N(HNC) <sup>b</sup> 10 <sup>13</sup> cm <sup>-2</sup>	N(HC <sub>3</sub> N) 10 <sup>11</sup> cm <sup>-2</sup>	N(CH <sub>3</sub> CN) <sup>c</sup> 10 <sup>11</sup> cm <sup>-2</sup>	N(CH <sub>3</sub> NC) 10 <sup>11</sup> cm <sup>-2</sup>	N(CH <sub>2</sub> CN) 10 <sup>11</sup> cm <sup>-2</sup>
B0355	-17	4.3	2.13	0.29	0.077	<0.22		< 0.18	< 1.5
	-14	5.0	<0.32	0.09	0.017				
	-10	4.8	3.35	0.36	0.123				
	-8	3.8	0.76	0.17	0.030				
	-4	4.0	<0.32	0.12	0.037				
	-all	22	6.6	1.05	0.28	<0.60	1.7(0.2)	<0.37	< 2.5
B0415		45	15.78	2.480	0.554	0.93(0.21)	3.9(0.3)	<0.44	< 2.4
B2200		8.7	3.29	0.450	0.074	<0.26	0.7(0.1)	<0.20	< 1.3
B2251		1.0	0.20	0.023	0.008	<0.49	<0.7	<0.52	< 3.0
TMC-1/10 <sup>d</sup>		10	3	2	2	60	10		50
TMC-1/10 <sup>e</sup>						234	4		38
consensus		10 – 20 <sup>i</sup>	3	2	2	120	6		44
B1b/10 <sup>g</sup>		≥ 60	6	5	2	2	0.1		
HH-PDR <sup>h</sup>						2.5	100	15	
HH-core <sup>h</sup>						5	5	<5	
Orion Bar <sup>j</sup> /10		30	2.5	0.34	0.4	3	7		

<sup>a</sup> all upper limits are 3 $\sigma$ <sup>b</sup> N(CN), N(HCN) and N(HNC) from Liszt & Lucas (2001)<sup>c</sup> Sum of N(CH<sub>3</sub>CN) K=0 and K=1<sup>d</sup> Ohishi et al. (1992) whose tables must be interpreted with N(H<sub>2</sub>) = 10<sup>22</sup> cm<sup>-2</sup><sup>e</sup> Gratier et al. (2016)<sup>g</sup> Loison et al. (2017) and Daniel et al. (2013)<sup>h</sup> Horsehead nebula values from Pety et al. (2012), Gratier et al. (2013) and Guzmán et al. (2015)<sup>i</sup> N(H<sub>2</sub>) ≥ 2 × 10<sup>22</sup> cm<sup>-2</sup> beam-averaged on 1' scales is given by Fehér et al. (2016)<sup>j</sup> Cuadrado et al. (2017)**Table 6.** Column densities for oxygen-bearing molecules<sup>a</sup>

Target	$\nu$ km s <sup>-1</sup>	N(H <sub>2</sub> ) 10 <sup>20</sup> cm <sup>-2</sup>	N(HNCO) 10 <sup>11</sup> cm <sup>-2</sup>	HCOOH 10 <sup>11</sup> cm <sup>-2</sup>	H <sub>2</sub> COH <sup>+</sup> 10 <sup>11</sup> cm <sup>-2</sup>
B0355	-17	4.3	<1.3	<1.5	<2.0
	-14	5.0			
	-10	4.8			
	-8	3.8			
	-4	3.8			
	-all	22	<3.1	<3.2	<4.5
B0415		45	<3.0	<3.1	<5.2
B2200		8.7	<1.1	<1.3	<1.6
B2251		1.0			<4.1
TMC-1/10 <sup>d</sup>		10	2	< 2	
TMC-1/10 <sup>e</sup>			11		
consensus		10-20 <sup>f</sup>	4.7	< 2	

<sup>d</sup> TMC-1 values from Ohishi et al. (1992)<sup>e</sup> TMC-1 values from Gratier et al. (2016)<sup>f</sup> N(H<sub>2</sub>) ≥ 2 × 10<sup>22</sup> cm<sup>-2</sup> beam-averaged on 1' scales according to Fehér et al. (2016)

Loison, J.-C., Agúndez, M., Wakelam, V., et al. 2017, Mon. Not. R. Astron. Soc., 470, 4075

Lucas, R., &amp; Liszt, H. 1998, A&amp;A, 337, 246

Lucas, R., &amp; Liszt, H. S. 1996, A&amp;A, 307, 237

—, 2000, A&amp;A, 355, 327

Maier, J. P., Walker, G. A. H., Bohlender, D. A., et al. 2011, ApJ, 726, 41

Majumdar, L., Das, A., &amp; Chakrabarti, S. K. 2014, A&amp;A, 562, A56

Marscher, A. P., Moore, E. M., &amp; Bania, T. M. 1993, ApJ, 419, L101

Mookerjee, B., Hassel, G. E., Gerin, M., et al. 2012, A&amp;A, 546, A75

Nash, A. G. 1990, Astrophys. J., Suppl. Ser., 72, 303

Ohishi, M., Irvine, W., &amp; Kaifu, N. 1992, in Astrochemistry of cosmic phenomena: proceedings of the 150th Symposium of the International Astronomical Union, held at Campos do Jordao, Sao Paulo, Brazil, August 5-9, 1991. Dordrecht: Kluwer, ed. P. D. Singh, 171–172

Ohishi, M., &amp; Kaifu, N. 1998, Faraday Discussions, 109, 205

Oka, T., Thorburn, J. A., McCall, B. J., et al. 2003, ApJ, 582, 823

Pety, J., Gratier, P., Guzmán, V., et al. 2012, A&amp;A, 548, A68

Riquelme, D., Bronfman, L., Mauersberger, R., et al. 2017, ArXiv e-prints, arXiv:1709.02464

Sakai, N., Saruwatari, O., Sakai, T., Takano, S., &amp; Yamamoto, S. 2010, A&amp;A, 512, A31+

Satta, M., Gianturco, F. A., Carelli, F., &amp; Wester, R. 2015, ApJ, 799, 228

Schlegel, D. J., Finkbeiner, D. P., &amp; Davis, M. 1998, ApJ, 500, 525

Sheffer, Y., Rogers, M., Ferman, S. R., et al. 2008, ApJ, 687, 1075

Snow, T. P., &amp; McCall, B. J. 2006, Ann. Rev. Astrophys. Astron., 44, 367

Sofia, U. J., Lauroesch, J. T., Meyer, D. M., &amp; Cartledge, S. I. B. 2004, ApJ, 605, 272

Thiel, V., Belloche, A., Menten, K. M., Garrod, R. T., &amp; Müller, H. S. P. 2017, A&amp;A, 605, L6

Valdivia, V., Godard, B., Hennebelle, P., et al. 2017, A&amp;A, 600, A114

Liszt, H. S., Pety, J., &amp; Lucas, R. 2008, A&amp;A, 486, 493

—, 2010, A&amp;A, 518, A45

**Table 7.** Comparison with Galactic Center and Scutum Arm diffuse clouds of Thiel et al. (2017)

Species	TMC-1 cm <sup>-2</sup>	B2200 cm <sup>-2</sup>	GC 1 cm <sup>-2</sup>	GC 2 cm <sup>-2</sup>	GC 3 cm <sup>-2</sup>	Scutum cm <sup>-2</sup>
H <sup>13</sup> CO <sup>+</sup>	1.3×10 <sup>12</sup> <sup>a</sup>	0.042×10 <sup>12</sup> <sup>a</sup>	1.5×10 <sup>12</sup>	8×10 <sup>12</sup>	4×10 <sup>12</sup>	0.6×10 <sup>12</sup>
<i>c</i> -C <sub>3</sub> H <sub>2</sub>	2.0×10 <sup>13</sup>	0.150×10 <sup>13</sup>	0.5×10 <sup>13</sup>	2×10 <sup>13</sup>	1×10 <sup>13</sup>	0.8×10 <sup>13</sup>
CH <sub>3</sub> OH	0.2×10 <sup>14</sup>	< 0.005 × 10 <sup>14</sup>	4×10 <sup>14</sup>	4×10 <sup>14</sup>	2×10 <sup>14</sup>	0.6×10 <sup>14</sup>
CH <sub>3</sub> CN	0.4×10 <sup>13</sup>	0.007×10 <sup>13</sup>	1×10 <sup>13</sup>	2×10 <sup>13</sup>	< 6 × 10 <sup>13</sup>	1.4×10 <sup>13</sup>
HC <sub>3</sub> N	13×10 <sup>13</sup>	< 0.004 × 10 <sup>13</sup>	< 3 × 10 <sup>13</sup>	60×10 <sup>13</sup>	< 3 × 10 <sup>13</sup>	< 2.5 × 10 <sup>13</sup>

<sup>a</sup> N(H<sup>13</sup>CO<sup>+</sup>) = N(HCO<sup>+</sup>)/62

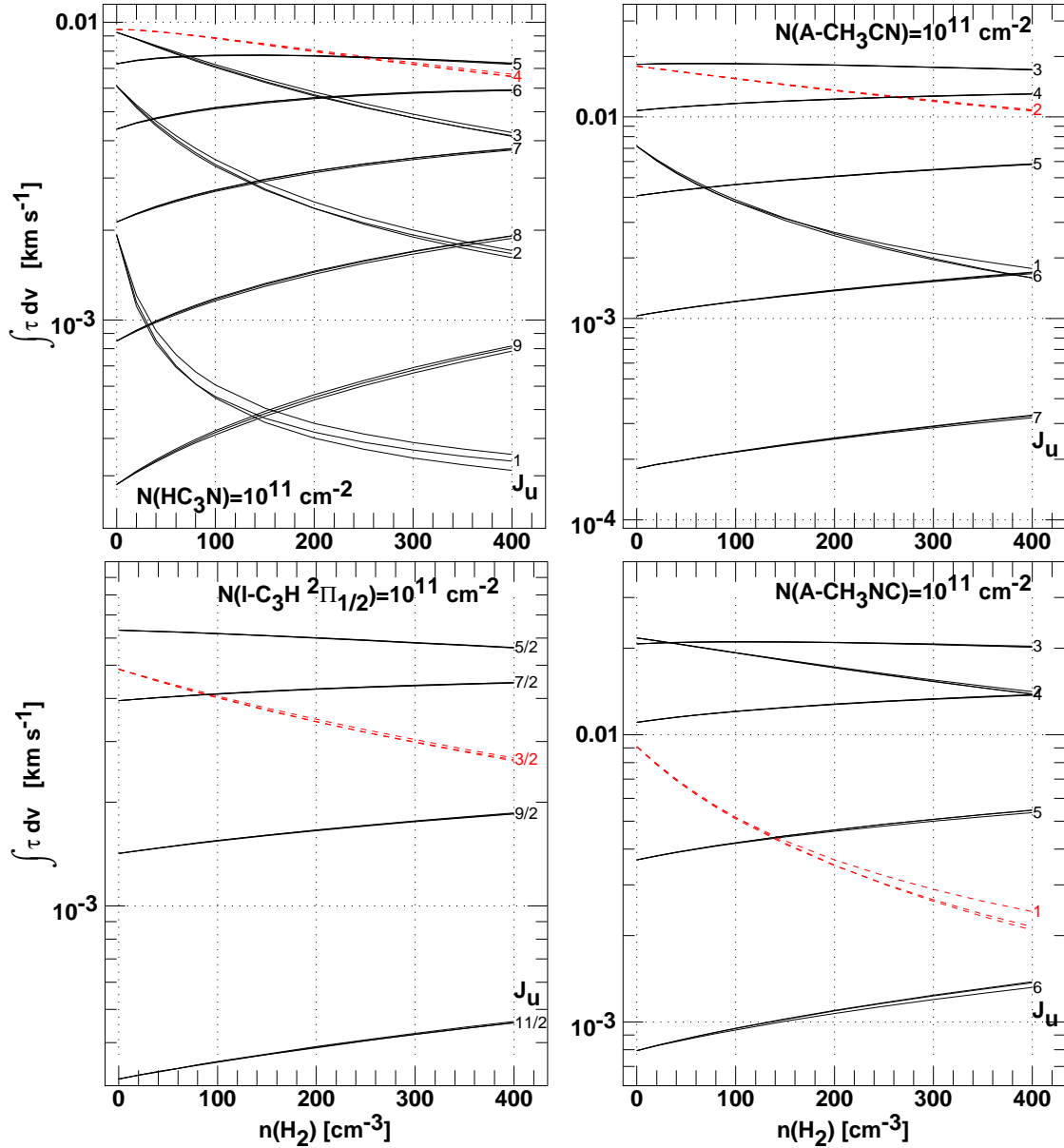


**Figure A1.** Integrated optical depth for rotational transitions of four molecules observed in the course of this work, assuming a column density of 10<sup>11</sup> cm<sup>-2</sup> in each case. The plots show the integrated optical depth of transitions whose upper-level quantum number is shown at the right of each series of three curves. The three curves for each transition correspond to calculations at kinetic temperatures of 20, 40 and 60 K and are often indistinguishable. The excitation calculations include H<sub>2</sub> and electrons for HC<sub>3</sub>N and He, H<sub>2</sub> and electrons for CH<sub>3</sub>CN, and only electrons otherwise, assuming an electron fraction  $n(e)/n(\text{H}_2) = 3 \times 10^{-4}$ . The transition observed in this work is shown in red, dashed lines.

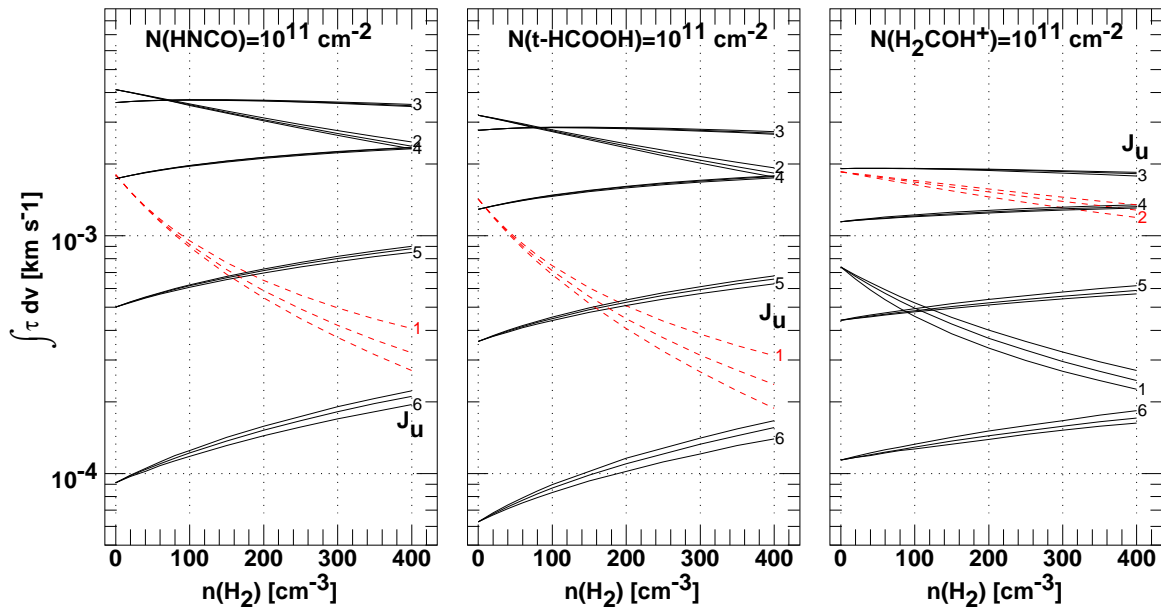


**Figure A2.** Integrated optical depth for rotational transitions of three oxygen-bearing molecules observed in the course of this work, assuming a column density of  $10^{11}$  cm<sup>-2</sup> in each case. The plots show the integrated optical depth of transitions whose upper-level quantum number is shown at the right of each series of three curves. The three curves correspond to calculations at kinetic temperatures of 20, 40 and 60 K. The calculations include electron excitation only, assuming an electron fraction  $n(e)/n(\text{H}_2) = 3 \times 10^{-4}$ . The transition observed in this work is shown in red, dashed lines.

Visser, R., van Dishoeck, E. F., & Black, J. H. 2009, A&A, 503, 323

Watson, W. D., Anicich, V. G., & Huntress, W. T., J. 1976, ApJ, 205, L165

Weselak, T., Galazutdinov, G., Beletsky, Y., & Krelowski, J. 2009, A&A, 499, 783

Weselak, T., Galazutdinov, G. A., Beletsky, Y., & Krelowski, J. 2010, Mon. Not. R. Astron. Soc., 402, 1991

Zuckerman, B., Ball, J. A., & Gottlieb, C. A. 1971, ApJ, 163, L41



